Zn-impurity effects on quasiparticle scattering in $La_{2-x}Sr_xCuO_4$ studied by angle-resolved photoemission spectroscopy

T. Yoshida,[1] Seiki Komiya,[2] X. J. Zhou,[3] K. Tanaka,[3] A. Fujimori,[1] Z. Hussain,[4] Z.-X. Shen,[3] Yoichi Ando,[5] H. Eisaki,[6] and S. Uchida[1]

[1]*Department of Physics, University of Tokyo, Bunkyo-ku, Tokyo 113-0033, Japan*

[2]*Central Research Institute of Electric Power Industry, Komae, Tokyo 201-8511, Japan*

[3]*Department of Applied Physics and Stanford Synchrotron Radiation Laboratory, Stanford University, Stanford, California 94305, USA*

[4]*Advanced Light Source, Lawrence Berkeley National Laboratory, Berkeley, California 94720, USA*

[5]*Institute of Scientific and Industrial Research, Osaka University, Ibaraki, Osaka 567-0047, Japan*

[6]*National Institute of Advanced Industrial Science and Technology, Tsukuba 305-8568, Japan*

(Received 11 August 2009; revised manuscript received 19 November 2009; published 18 December 2009)

Angle-resolved photoemission measurements were performed on Zn-doped $La_{2-x}Sr_xCuO_4$ to investigate the effects of Zn impurities on the low-energy electronic structure. The Zn-impurity-induced increase in the quasiparticle width in momentum distribution curves (MDCs) is approximately isotropic on the entire Fermi surface and energy independent near the Fermi level (E_F). The increase in the MDC width is consistent with the increase in the residual resistivity due to the Zn impurities if we assume the carrier number to be $1-x$ for $x=0.17$ and the Zn impurity to be a potential scatterer close to the unitarity limit. For $x=0.03$, the residual resistivity is found to be higher than that expected from the MDC width, and the effects of antiferromagnetic fluctuations induced around the Zn impurities are discussed. The leading edges of the spectra near $(\pi,0)$ for $x=0.17$ are shifted toward higher energies relative to E_F with Zn substitution, indicating a reduction in the superconducting gap.

DOI: 10.1103/PhysRevB.80.245113 PACS number(s): 71.18.+y, 74.25.Jb, 74.72.Dn, 79.60.−i

I. INTRODUCTION

Zn substitution for Cu atoms in the CuO_2 planes for the high-T_c cuprates causes a dramatic reduction in T_c and thus may offer an opportunity to characterize the nature of the superconducting states in the cuprates. Zn is a nonmagnetic impurity with a closed *d* shell and produces a large in-plane residual resistivity while the temperature slope of the resistivity is unchanged.[1] Quantitative analysis of the residual resistivity indicates that the Zn impurity acts as a potential scatterer in the unitarity limit. To understand the microscopic mechanism of the scattering by the Zn impurities, the local information around the Zn impurities has been extensively studied. Reduction in superfluid density by Zn impurities were detected by μSR (muon spin relaxation, Ref. 2) and a "Swiss cheese" model, in which nonsuperconductivity islands are induced around the Zn impurities, was proposed to explain the reduction in the superconducting fraction proportional to the Zn concentration. This model is consistent with the observation by scanning tunneling microscopy (STM) that the superconductivity is locally destroyed by Zn impurities.[3] Also, according to NMR studies, it was found that antiferromagnetic moment is induced around the Zn impurity.[4] While these experimental results have given insight into the local electronic structure around the impurity, Zn-impurity effects in momentum space, which are more directly related to the transport properties, are still poorly understood.

In order to elucidate details of impurity scattering in momentum space as well as the mechanism of the reduction in T_c induced by impurity, direct observation of the quasiparticle (QP) under the influence of Zn impurities should give useful information. Previous angle-resolved photoemission spectroscopy (ARPES) studies indicated that in $Bi_2Sr_2CaCu_2O_{8+\delta}$ (Bi2212) Zn and Ni impurities reduce the coupling strength to boson excitation, which leads the "kink" in the QP dispersion.[5,6] Also, the depression of the superconducting coherence peak by Zn impurities has been observed,[5–8] consistent with the decrease in the superfluid density.[2] In this work, we shall focus on the impurity effects on the QP in $La_{2-x}Sr_xCuO_4$ (LSCO), particularly, on the relationship between the T_c and the observed increase in the widths of momentum distribution curves (MDCs) in relation to the scattering mechanism of QP in the normal state. In particular, the effects of antiferromagnetic fluctuations locally induced by the Zn impurities shall be discussed.

II. EXPERIMENT

High-quality single crystals of Zn-doped and Zn-free LSCO were grown by the traveling-solvent floating-zone method. Figure 1 shows the temperature dependence of the electrical resistivity ρ and the Hall coefficient R_H of samples studied in the present work. The Zn-free and 2% Zn-doped samples with hole content of $x=0.17$ have critical temperatures (T_c's) of 40 and 22 K, respectively. The Zn-free and 3% Zn-doped $x=0.03$ samples are nonsuperconducting. With Zn doping, the residual resistivity increases for both $x=0.03$ and 0.17 samples, while the temperature slope of ρ does not change with the Zn impurities for the $x=0.17$ sample. The "carrier number" defined by $(eR_H)^{-1}$ for $x=0.03$ is close to the nominal hole concentration, but decreases by ~20% with 3% Zn doping. The ARPES measurements were carried out at beamline 10.0.01 of the Advanced Light Source (ALS) and beamline 5-4 of Stanford Synchrotron Radiation Laboratory (SSRL), using incident photons with energies of 55.5 and 22.4 eV, respectively. The total-energy resolution was about 15 meV (SSRL) or 20 meV (ALS). The momentum

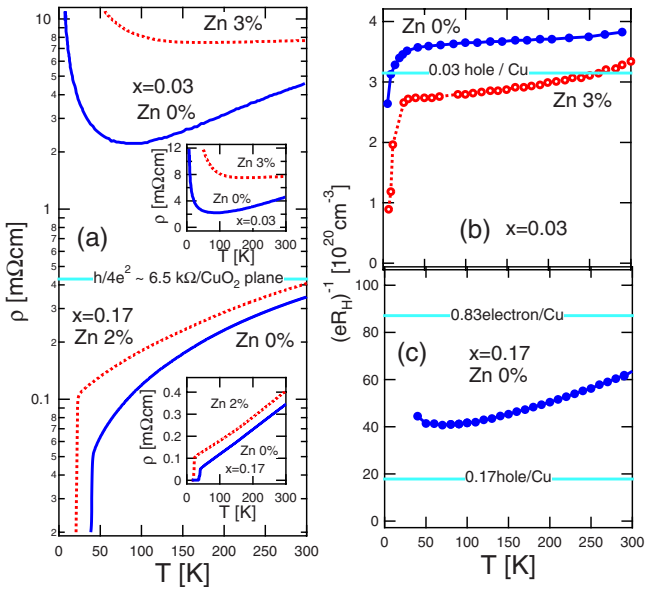

FIG. 1. (Color online) Transport properties of Zn-doped LSCO samples studied in this work. (a) Electrical resistivity ρ. Insets show ρ on linear scale. (b),(c) Hall coefficient R_H.

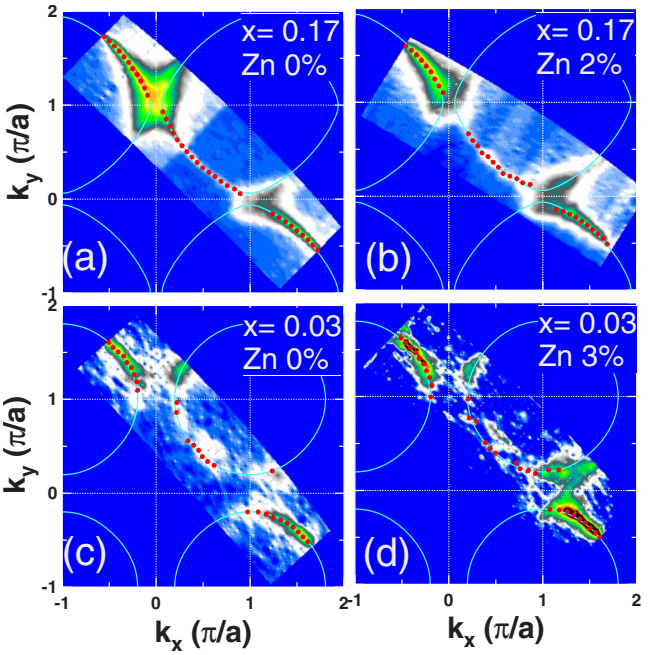

FIG. 2. (Color online) k-space spectral weight mapping at E_F for $La_{2-x}Sr_xCu_{1-y}Zn_yO_4$. Dots indicate k_F positions determined by MDC peaks at E_F. Solid curves show the Fermi surface fitted to the tight-binding model.

resolutions at ALS and SSRL are 0.02π and 0.01π in units of $1/a$, respectively, where $a=3.8$ Å is the lattice constant. The samples were cleaved *in situ* and measurements were performed at about 20 K (ALS) or 10 K (SSRL). In the measurements at ALS, the electric vector **E** of the incident photons lied within the CuO_2 plane, 45° rotated from the Cu-O direction and was parallel to the Fermi-surface segment in the nodal region. This measurement geometry enhances dipole matrix elements in this **k** region because the wave function has x^2-y^2 symmetry.[9] **E** in the measurements at SSRL was nearly parallel to the Cu-O direction.

III. RESULTS AND DISCUSSION

A. Zn-impurity effects on the quasiparticle

First, in order to see the effects of Zn impurities on the shape of the Fermi surface, momentum-space spectral weight mapping at the Fermi level (E_F) is shown in Fig. 2. We have determined the Fermi momentum (k_F) of the (underlying) Fermi surfaces by using the peak positions of the MDCs, as represented by dots.[10] The k_F positions thus determined, which designate the shape of the Fermi surfaces, could be well fitted to the Fermi surface of the tight-binding model as shown by solid curves. Both for $x=0.03$ and 0.17, the tight-binding parameters are almost identical between the Zn-doped and Zn-free samples ($t'/t=-0.120$, $t''/t=0.10$ for $x=0.03$ and $t'/t=-0.135$, $t''/t=0.075$ for $x=0.17$), indicating that the Zn substitution does not change the overall electronic structure and the hole concentration appreciably. Although R_H for $x=0.03$ shown in Fig. 1(b) suggests a decrease in the hole concentration with Zn doping by ~20%, we could not detect this signature in the present experiment since the corresponding change is a very small portion of the Fermi-surface area $1+x$ ($\ll 1\%$).

Nevertheless, Zn-impurity effects are clearly seen in the spectral line shapes of the energy distribution curves (EDCs). Figure 3 shows EDCs in the nodal direction $[(0,0)$-$(\pi,\pi)]$ in the second Brillouin zone. Clear QP peaks are observed near E_F in the Zn 0% $x=0.17$ and 0.03 samples [Figs. 3(a) and 3(c), respectively]. With Zn substitution, the peak is significantly depressed [Figs. 3(b) and 3(d)]. As indicated by vertical arrows, a characteristic dip at ~70 meV, which corresponds to the kink is prominent for the $x=0.03$ spectra. The dip feature still remains at almost the same binding energy with Zn doping.

To clarify the impurity effects on the QP spectral weight, the EDCs at k_F have been symmetrized with respect to E_F as shown in Fig. 3(e). These spectra have been normalized to the spectral weight between −0.2 and −0.1 eV below E_F. For both the Zn-free and Zn-doped $x=0.17$ samples, the symmetrized EDCs show a clear QP peak at the k_F point although the QP intensity decreases with Zn doping. The existence of a clear QP peak even for the Zn-doped sample may be related with the persistence of superconductivity with $T_c=22$ K. On the other hand, the QP peak is strongly depressed in the Zn-doped $x=0.03$ sample. Particularly, the symmetrized EDCs at k_F show a shallow dip at E_F, indicating the destruction of the nodal QP and a possible pseudogap opening. Note that the pseudogap on the energy scale of ~10 meV caused by charge localization was observed in the optical conductivity measurement of LSCO ($x=0.03$) at low temperature.[11] The observed pseudogaplike feature of similar magnitude in the EDC of the $x=0.03$ Zn 3% sample would therefore be related to the localization behavior at low temperature of the electrical resistivity as seen in Fig. 1. The integrated MDC spectra along the nodal direction in Fig. 3(f) for both hole concentrations also show the suppression of the spectral weight by the Zn impurities.

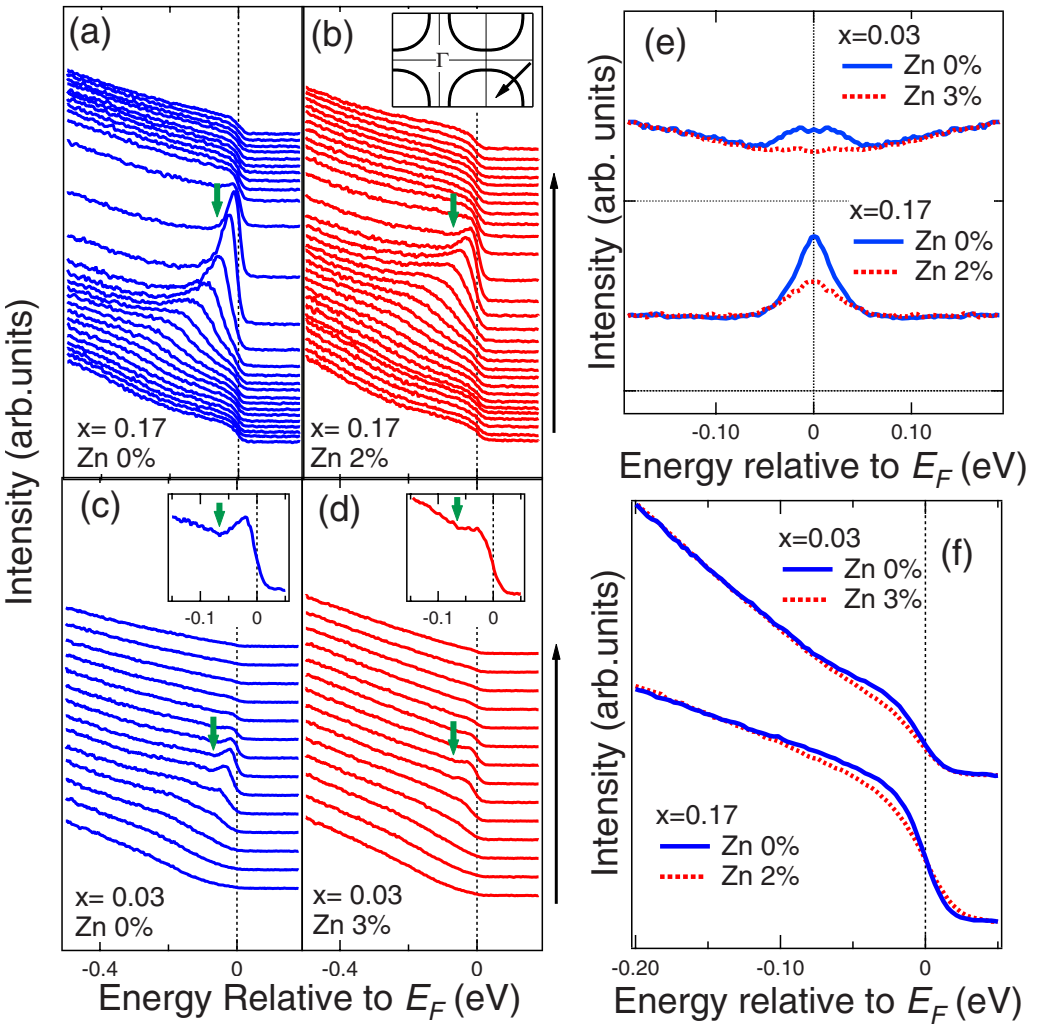

FIG. 3. (Color online) ARPES spectra of $La_{2-x}Sr_xCu_{1-y}Zn_yO_4$ in the nodal direction of the second Brillouin zone. (a)–(d) EDCs corresponding to the cut shown by an arrow in the inset. Arrows in the panels indicate the energy positions of a dip in the spectral line shape. Insets in (c) and (d) show EDCs near k_F with clear dips. (e) Symmetrized EDCs at k_F with respect to E_F. (f) EDCs integrated along the nodal direction. The spectra in (e) and (f) have been normalized to the integrated spectral weight between −0.2 and −0.1 eV.

In Fig. 4, we summarize the dispersion of the QP peak in MDCs and the energy dependence of the MDC width in the nodal direction. Both the $x=0.03$ and 0.17 samples show a kink at ~70 meV [Figs. 4(a) and 4(b)]. In Fig. 4(c), one can confirm that the Fermi velocity for the Zn-free samples does not change with hole doping, i.e., the universal Fermi velocity.[12] By contrast, the slopes of the energy dispersions near E_F slightly increases with Zn doping as shown in Figs. 4(a) and 4(b). Figure 4(d) indicates that the slope of the dispersion within ~20 meV of E_F becomes steeper in $x=0.03$ Zn 3%, which however may be an artifact due to the (pseudo)gap opening [Fig. 3(e)]. Indeed, such an effect is absent in the $x=0.17$ samples [Fig. 4(e)].

Next, let us look at the effect of Zn impurities on the MDC width in the nodal direction [Figs. 4(f) and 4(g)]. The MDC width shows a characteristic drop below the kink energy of ~70 meV, especially for the $x=0.03$ samples, indicating a reduction in the scattering rate of QP by collective modes below the mode energy. Below the kink energy, the Zn-induced increase in the MDC width is energy independent as clearly indicated by the difference between the Zn-doped and Zn-free data. Since the MDC width Δk increases with decreasing mean free path l through $\Delta k=1/l$ the extra scattering due to the impurity, the energy-independent increase in the MDC width is consistent with the temperature-independent increase in the resistivity caused by the Zn impurities.

In order to see the momentum dependence of the increase in the MDC on the Fermi surface, the MDC widths at various k_F's are shown in Fig. 5. The energy dependence of the MDC width is compared between the Zn-doped and Zn-free samples in Figs. 5(a) and 5(b), and the MDC width at E_F is plotted in Figs. 5(c) and 5(d) as a function of the Fermi angle α. Also, the differences of the MDC width between the Zn-free and Zn-doped samples are plotted on the same panels. These plots indicate that the increase in the MDC width by the Zn impurity is almost isotropic on the Fermi surface. Thus, on the low-energy scale (<70 meV), the contribution of the impurity to the MDC width is energy and momentum independent, indicating that the Zn impurity is a nearly static

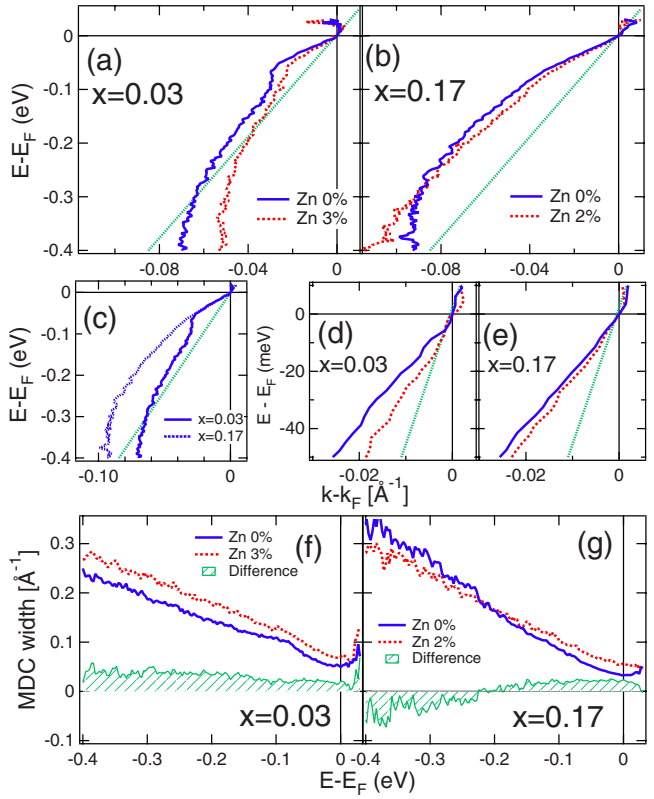

FIG. 4. (Color online) Quasiparticle peak in MDCs in the nodal direction of $La_{2-x}Sr_xCu_{1-y}Zn_yO_4$. (a),(b) Energy dispersions determined by MDC peaks. (c) Comparison between the Zn-free $x=0.03$ and 0.17 samples. (d),(e) Enlarged plot near E_F of (a) and (b), respectively. (f),(g) Energy dependence of the MDC width in the nodal direction.

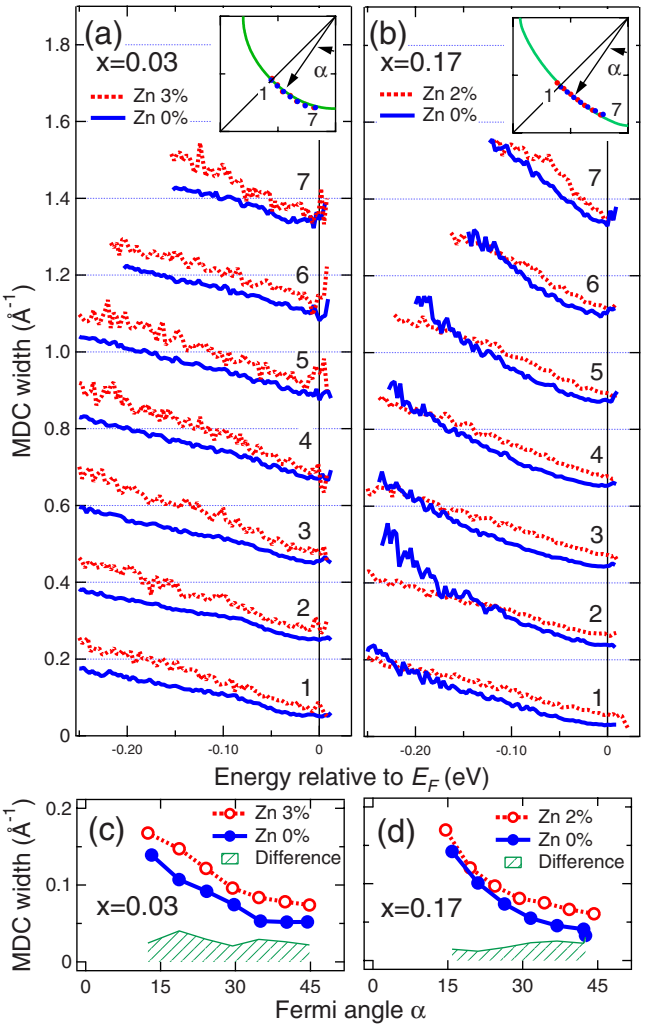

FIG. 5. (Color online) MDC widths at various k_F points on the Fermi surface of $La_{2-x}Sr_xCu_{1-y}Zn_yO_4$. (a),(b) Energy dependence of the MDC width for $x=0.03$ and 0.17, respectively. The data are shifted by 0.2 $Å^{-1}$ between different momenta. (c),(d) MDC width at E_F as a function of Fermi angle α. Differences in the width between the Zn-free and Zn-doped samples are also plotted.

and isotropic scatterer. As a result of the momentum-independent increase in the MDC width, the relative increase in the MDC width for 2–3 % Zn substitution is 10–20 % in the antinode direction and 50–100 % in the node direction. Because the pseudogap size mainly determines the c-axis transport properties in underdoped samples, the small relative increase in the MDC width in the antinodal region compared to the nodal region may explain the fact that the out-of-plane transport is less affected by the Zn impurities than the in-plane transport.[13]

B. Comparison with transport properties

Since the MDC width is equal to the inverse of the mean free path, here, we shall compare the transport properties with the MDC width deduced from the present ARPES results. The mobility $\mu=e\tau/m^*$ can be derived from the in-plane resistivity $\rho=m^*/ne^2\tau$ and the carrier density n if the Drude formula is assumed. We have assumed that n is given by $n=x$ and $n=1-x$ for $x=0.03$ and 0.17, respectively, because the Hall coefficient[14,15] $R_H=1/ne$ as well as the residual resistivity of Zn-doped LSCO (Ref. 1) shows a crossover from $n\sim x$ to $n\sim 1-x$ around $x=0.1$. From the ARPES data, the inverse mobility can be calculated using the formula $\mu^{-1}=m^*/e\tau=m^*v_F/ev_F\tau=\hbar k_F\Delta k/e$, where Δk is the MDC width. As the observed MDC width is influenced by the finite angular and energy resolutions, we have subtracted the angular broadening ~ 0.01 $Å^{-1}$ from the measured MDC widths. When the Fermi surface has a pseudogap as in the underdoped region, since the QPs in the node region dominate the in-plane transport, the evaluated μ^{-1} would be that of the node region. As for the slightly overdoped $x=0.17$ samples, too, the scattering rate is the lowest in the nodal region, as can be seen from the smallest MDC width in this region [see Fig. 5(d)]. Therefore, the evaluated μ^{-1} is largely determined by the nodal QPs.

In Fig. 6, we compare the Zn-induced increase in the inverse mobility μ^{-1} obtained from the transport and present ARPES results.[16] From the measurements of the electrical resistivity ρ of the present samples, the inverse mobility $\mu^{-1}=ne\rho$, with $n=x$ ($x=0.03$) or $n=1-x$ ($x=0.17$), is found to increase with Zn doping by 0.16 and 0.098 V s/cm^2 for $x=0.03$ and 0.17, respectively, at 300 K. From the MDC width at E_F in the nodal direction (Fig. 4), the Zn-induced increases in Δk are 0.022 and 0.020 $Å^{-1}$ for the $x=0.03$ and

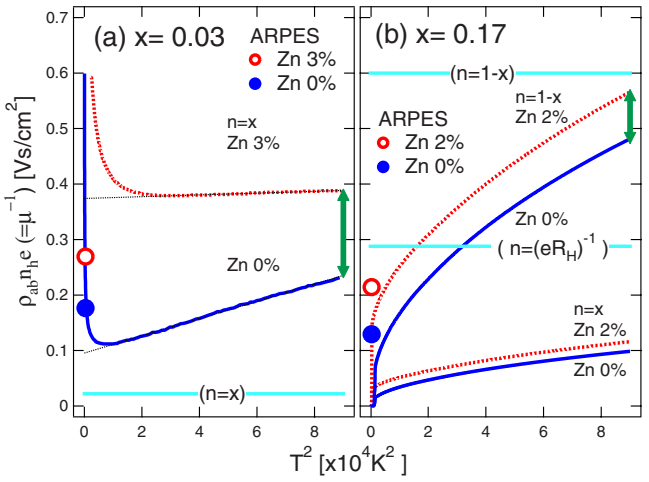

FIG. 6. (Color online) Comparison of the inverse mobility obtained from the electrical resistivity and those estimated from ARPES results for $La_{2-x}Sr_xCu_{1-y}Zn_yO_4$. Inverse mobility corresponding to the universal resistance $h/4e^2$ and assumed carrier number (n in parentheses) are shown by horizontal lines. Arrows indicate the increase in the inverse mobility at $T=300$ K, which is compared with the ARPES results.

0.17 samples, respectively. Using the increase in Δk and the formula $\mu^{-1}=\hbar k_F \Delta k/e$, the increases in μ^{-1} for $x=0.03$ and 0.17 samples are calculated to be 0.093 and 0.085, respectively. Here, $k_F \sim 0.64$ Å^{-1} measured from (π,π) was deduced from ARPES. Therefore, for the $x=0.17$ samples, the obtained Zn-induced increase in the μ^{-1} values from the transport and ARPES results are quantitatively consistent if we assume $n=1-x$. On the other hand, for the $x=0.03$ samples, the increase in μ^{-1} from ARPES is smaller than that estimated from the transport.

In general, transport and ARPES measurements detect different scattering processes of QP in different weights. The scattering rate $1/\tau_{\rm tr}$ by impurities in transport is given by $1/\tau_{\rm tr} \propto \frac{1}{2}\int v(\mathbf{k}-\mathbf{k}')(1-\cos\theta)d\theta$, where θ is the scattering angle and $v(\mathbf{q})$ is the scattering potential.[17] Because of the factor $1-\cos\theta$ in the integrand, the main scattering process stems from backward scattering. On the other hand, the scattering rate in ARPES $(1/\tau_{\rm ARPES})$ is $1/\tau_{\rm ARPES}=2Z\,{\rm Im}\,\Sigma \propto \frac{1}{2}\int v(\mathbf{q})d\theta$, where Σ is the self-energy and Z is the renormalization factor, indicating that both backward scattering and forward scattering equally contribute. It should be noted that, in the unitarity limit, $1/\tau_{\rm tr}$ and $1/\tau_{\rm ARPES}$ should be the same due to the $\mathbf{q}$ independence of the scattering amplitude. Since the Zn-induced increase in μ^{-1} from the transport (assuming $n=1-x$) and ARPES results for $x=0.17$ samples show almost the same value of ~ 0.09 V s/cm^2, one can conclude that the scattering by the Zn impurities in the $x=0.17$ samples are in the unitarity limit. This is consistent with the in-plane resistivity results[1] and with the conclusion reached by an STM study.[3]

For the $x=0.03$ samples, on the other hand, the increase in μ^{-1} from ARPES is smaller than that from transport (which is extrapolated from the high-temperature region in order to eliminate the localization effect). This cannot be understood within the unitary scattering picture. Here, let us consider the effects of antiferromagnetic correlations induced around the impurity atom.[4] Theoretically, vertex correction from the antiferromagnetic fluctuations may cause an enhancement of the resistivity compared to that calculated based on the Boltzmann equation.[18] Since the present estimate from the ARPES data is based on the Boltzmann transport theory, the smaller μ^{-1} estimated from ARPES than that from the transport indicates that the QP scattering rate has a peculiar momentum dependence with a maximum occurring in the backward scattering direction. Such a situation may be realized if scattering by the low-energy antiferromagnetic fluctuations induced by the Zn impurities is dominant in the QP scattering in the $x=0.03$ samples.

In two-dimensional (2D) metals like high-T_c cuprates, whether a dirty system become a superconductor or not is determined by the normal-state critical sheet resistance.[19] In both Zn 0% and 3% $x=0.03$ samples, it is clear that the inverse mobilities obtained by the ARPES and transport studies are much higher than critical universal 2D value and, therefore, the system indeed goes into the localization phase. This explains the absence of superconductivity in the Zn-free $x=0.03$ samples, although it shows a clear QP in the vicinity of E_F near the node direction. It is likely that a tiny gap is opened in the nodal direction [Fig. 3(e)], as pointed out in a previous report on the lightly doped cuprates.[20] With Zn doping, the QP peak is significantly depressed as shown in Figs. 3(e) and 3(f), a signature of carrier localization which starts at higher temperature. Note that a pseudogap on the low-energy scale of ~ 10 meV was observed in the optical conductivity measurement and indicated localization at low temperatures.[11] In the Zn 2% $x=0.17$ samples, the inverse mobility obtained by ARPES is lower than the universal resistivity, which accords with the persistence of the superconductivity in this sample. One can infer that, with a few more percent Zn doping, the inverse mobility would reach that of the universal resistivity and the system would enter the nonsuperconducting phase.

C. Zn-impurity effects in the antinodal region

Finally, we discuss Zn-impurity effects on the spectra in the antinodal region, where the opening of the superconducting gap is expected below T_c. Figure 7 shows EDCs along the $(\pi,0)$-(π,π) line of the $x=0.17$ samples measured at SSRL. At the k_F point with $k_y \sim \pm 0.1\pi$, the EDCs of the Zn-doped sample are slightly shifted toward higher energies relative to E_F compared to the Zn-free sample. Because the pseudogap state has been reported to be stabilized by out-of-plane disorder,[21] if in-plane and out-of-plane disorders have similar effects on the pseudogap, the observed shift is unlikely to be a reduction in the pseudogap. Instead, the shift may be understood as a reduction in the superconducting gap because such a reduction by Zn impurity has also been observed in Zn-doped Bi2212.[8] However, the decrease in the gap by Zn doping is only 1–2 meV, which is much smaller than that (~ 4 meV) expected from the decrease in T_c by 20 K. Furthermore, the observed gap size is too small compared with that estimated from the d-wave BCS theory $\Delta \sim 8$ meV for the Zn-free samples with $T_c \sim 40$ K.[22] Note

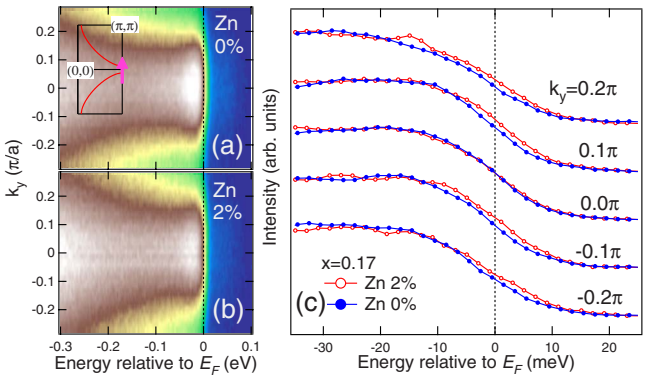

FIG. 7. (Color online) Zn-impurity effects on the spectra around $(\pi,0)$ for LSCO $x=0.17$ samples. (a) and (b) show intensity plots in the E-k_y space (with $k_x=\pi$ fixed) for Zn 0% and 2%, respectively. Inset shows cut direction. (c) Comparison of the EDCs of Zn 0% and 2% samples. The EDCs at $k_y=\pm 0.1\pi$ show energy shifts of the spectra with Zn doping.

that, for $x=0.15$ samples, an indication of the leading edge gap of ~10 meV was reported in previous studies although no clear coherence peak was seen around $(\pi,0)$ (Ref. 23) even using higher-energy resolution than the present one. Therefore, the superconducting gap identified in this study may be opened on top of the pseudogap and hence is probably blurred compared to an ideal superconducting gap. More detailed systematic studies are necessary to characterize the weak superconductivity in the antinodal region.

IV. CONCLUSION

In summary, we have studied Zn-impurity effects on the near E_F electronic states of LSCO and discussed their relationship to the transport properties. We have observed an isotropic increase in the MDC width as well as the suppression of spectral weight in the low-energy part of the spectra. For slightly overdoped $x=0.17$, the increase in the MDC width is close to that expected from the unitary limit of the impurity scattering and explains the increase in the in-plane residual resistivity. For the lightly doped $x=0.03$, we found that the residual resistivity is larger than that expected from the MDC width. We propose that backward scattering due to antiferromagnetic fluctuations may be enhanced compared to forward scattering. We have confirmed that superconductor-to-localization behavior is caused by the increase in the MDC width up to the universal resistivity in the underdoped region.

ACKNOWLEDGMENTS

We are grateful to Y. Yanase for enlightening discussions. This work was supported by a Grant-in-Aid for Scientific Research in Priority Area "Invention of Anomalous Quantum Materials" and a Grant-in-Aid for Young Scientists from the Ministry of Education, Science, Culture, Sports and Technology, Japan. Y.A. was supported by KAKENHI Contracts No. 19674002 and No. 20030004. ALS is operated by the Department of Energy (DOE) Office of Basic Energy Science, Division of Materials Science. SSRL is operated by the DOE Office of Basic Energy Science Divisions of Chemical Sciences and Material Sciences.

[1] Y. Fukuzumi, K. Mizuhashi, K. Takenaka, and S. Uchida, Phys. Rev. Lett. **76**, 684 (1996).
[2] B. Nachumi, A. Keren, K. Kojima, M. Larkin, G. M. Luke, J. Merrin, O. Tchernyshöv, Y. J. Uemura, N. Ichikawa, M. Goto, and S. Uchida, Phys. Rev. Lett. **77**, 5421 (1996).
[3] S. H. Pan, E. W. Hudson, K. M. Lang, H. Eisaki, S. Uchida, and J. C. Davis, Nature (London) **403**, 746 (2000).
[4] M.-H. Julien, T. Fehér, M. Horvatić, C. Berthier, O. N. Bakharev, P. Ségransan, G. Collin, and J.-F. Marucco, Phys. Rev. Lett. **84**, 3422 (2000).
[5] K. Terashima, H. Matsui, D. Hashimoto, T. Sato, T. Takahashi, H. Ding, T. Yamamoto, and K. Kadowaki, Nat. Phys. **2**, 27 (2006).
[6] V. B. Zabolotnyy, S. V. Borisenko, A. A. Kordyuk, J. Fink, J. Geck, A. Koitzsch, M. Knupfer, B. Buchner, H. Berger, A. Erb, C. T. Lin, B. Keimer, and R. Follath, Phys. Rev. Lett. **96**, 037003 (2006).
[7] K. Terashima, T. Sato, K. Nakayama, T. Arakane, T. Takahashi, M. Kofu, and K. Hirota, Phys. Rev. B **77**, 092501 (2008).
[8] S. Nishina, T. Sato, T. Takahashi, S.-C. Wang, H.-B. Yang, H. Ding, and K. Kadowaki, J. Phys. Chem. Solids **63**, 1069 (2002).
[9] T. Yoshida, X. J. Zhou, M. Nakamura, S. A. Kellar, P. V. Bogdanov, E. D. Lu, A. Lanzara, Z. Hussain, A. Ino, T. Mizokawa, A. Fujimori, H. Eisaki, C. Kim, Z.-X. Shen, T. Kakeshita, and S. Uchida, Phys. Rev. B **63**, 220501(R) (2001).
[10] Shadow bands seen in the first Brillouin zone in Figs. 2(c) and 2(d) are not considered in the present analysis because these bands may be extrinsic structures. The origin of the "shadow band" is discussed by A. Koitzsch, S. V. Borisenko, A. A. Kordyuk, T. K. Kim, M. Knupfer, J. Fink, M. S. Golden, W. Koops, H. Berger, B. Keimer, C. T. Lin, S. Ono, Y. Ando, and R. Follath, Phys. Rev. B **69**, 220505(R) (2004), in terms of structural effects.
[11] M. Dumm, S. Komiya, Y. Ando, and D. N. Basov, Phys. Rev. Lett. **91**, 077004 (2003).
[12] X. J. Zhou, T. Yoshida, A. Lanzara, P. V. Bogdanov, S. A. Kellar, K. M. Shen, W. L. Yang, F. Ronning, T. Sasagawa, T. Kakeshita, T. Noda, H. Eisaki, S. Uchida, C. T. Lin, F. Zhou, J. W. Xiong, W. X. Ti, Z. X. Zhao, A. Fujimori, Z. Hussain, and Z. X. Shen, Nature (London) **423**, 398 (2003).
[13] K. Mizuhashi, K. Takenaka, Y. Fukuzumi, and S. Uchida, Phys. Rev. B **52**, R3884 (1995).
[14] Y. Ando, Y. Kurita, S. Komiya, S. Ono, and K. Segawa, Phys. Rev. Lett. **92**, 197001 (2004).
[15] S. Ono, S. Komiya, and Y. Ando, Phys. Rev. B **75**, 024515 (2007).
[16] If the surface qualities and the experimental conditions are nearly the same between the Zn-free and the Zn-doped samples,

the increase in the MDC width can be quantitatively attributed to by the Zn-impurity scattering.

[17] G. D. Mahan, *Many-Particle Physics*, 2nd ed. (Plenum, New York, 1990).

[18] H. Kontani, K. Kanki, and K. Ueda, Phys. Rev. B **59**, 14723 (1999).

[19] V. J. Emery and S. A. Kivelson, Phys. Rev. Lett. **74**, 3253 (1995).

[20] K. M. Shen, T. Yoshida, D. H. Lu, F. Ronning, N. P. Armitage, W. S. Lee, X. J. Zhou, A. Damascelli, D. L. Feng, N. J. C. Ingle, H. Eisaki, Y. Kohsaka, H. Takagi, T. Kakeshita, S. Uchida, P. K. Mang, M. Greven, Y. Onose, Y. Taguchi, Y. Tokura, Seiki Komiya, Yoichi Ando, M. Azuma, M. Takano, A. Fujimori, and Z.-X. Shen, Phys. Rev. B **69**, 054503 (2004).

[21] Y. Okada, T. Takeuchi, T. Baba, S. Shin, and H. Ikuta, J. Phys. Soc. Jpn. **77**, 074714 (2008).

[22] H. Won and K. Maki, Phys. Rev. B **49**, 1397 (1994).

[23] K. Terashima, H. Matsui, T. Sato, T. Takahashi, M. Kofu, and K. Hirota, Phys. Rev. Lett. **99**, 017003 (2007).